Available online at www.sciencedirect.com
SCIENCE DIRECT®
Bioorganic & Medicinal Chemistry 13 (2005) 463–471
Bioorganic & Medicinal Chemistry

Application of QSAR analysis to organic anion transporting polypeptide 1a5 (Oatp1a5) substrates

Mine Yarim,[a,*] Stefano Moro,[b] Robert Huber,[c] Peter J. Meier,[c] Chosei Kaseda,[d] Toru Kashima,[d] Bruno Hagenbuch[c] and Gerd Folkers[a]

[a]*Institute of Pharmaceutical Sciences, ETH Zurich, D-ANBI, Wintherthurerstrasse 190, CH-8057 Zurich, Switzerland*
[b]*Molecular Modeling Section, Department of Pharmaceutical Sciences, University of Padova, Via Marzolo, 5, 35131 Padova, Italy*
[c]*Division of Clinical Pharmacology and Toxicology, Department of Internal Medicine, University Hospital, CH-8091 Zurich, Switzerland*
[d]*Yamatake Corporation, 1-12-2 Kawana, Fujisawa-shi, Kanagawa 251-8522, Japan*

Received 13 August 2004; revised 4 October 2004; accepted 5 October 2004
Available online 2 November 2004

Abstract—Organic anion transporting polypeptide 1a5, Slco1a5 (previously called Oatp3, Slc21a7) is a multispecific transmembrane transport protein that belongs to the OATP/*SLCO* superfamily of solute carriers. It is expressed in several epithelial barriers such as the small intestine and the choroid plexus where it might play an important role in the disposition of numerous endogenous and exogenous organic compounds. Since the molecular basis of the multispecificity of Oatp1a5 is not known and the three-dimensional structure not solved yet, we used three-dimensional quantitative structure–activity relationship (3D-QSAR) techniques to obtain topological information on the substrate binding site of the protein. We aligned a heterogeneous data set of 18 Oatp1a5 substrates using the Genetic Algorithm Similarity Program (GASP) and performed comparative molecular field analysis (CoMFA) using this alignment. This resulted in a reasonable QSAR model including steric and electrostatic fields with a leave-one-out cross-validated r^2_{cv} value of 0.705 and a no-cross-validated regression coefficient r^2 value of 0.949. Based on the derived model we identified new potential Oatp1a5 substrates and confirmed their predicted apparent affinity values experimentally.

1. Introduction

Drug transporters are expressed in many tissues such as the intestine, liver, kidney, and brain. They play key roles in drug absorption, distribution, and excretion. In recent years, a number of important transporters have been cloned, and considerable progress has been made in understanding the molecular characteristics of individual transporters. It has now become clear that drug transporters are key determinants of the pharmacokinetic characteristics of numerous drugs as far as their intestinal absorption, tissue distribution, and elimination are concerned.[1]

Organic anion transporting polypeptides (rodents: Oatps, human: OATPs) belong to the *Slco*/*SLCO* gene superfamily[2] and mediate uptake of a wide variety of amphipathic compounds including bile salts, steroids and their conjugates, hormones, peptides, and various drugs.[3] Oatps/OATPs are important multispecific transporters and part of the overall body detoxification system. So far, the molecular basis for their multispecificity has not been characterized in any detail.

Oatp1a5 is a membrane protein of 670 amino acids with 12 predicted transmembrane domains.[4,5] Similar to other Oatps/OATPs, Oatp1a5 has a broad substrate specificity and might play an important role in the disposition of numerous amphipathic organic compounds including bile salts, hormones and their conjugates, prostaglandins, peptides, and drugs.[4–7] Since Oatps/OATPs are membrane proteins, their three-dimensional structure has not been resolved yet and the cause of their broad substrate specificities is not known. Therefore, we decided to use a ligand-based approach

Keywords: 3D-QSAR; CoMFA; Oatp1a5; Prediction of activity; Organic anion transporting polypeptide.
* Corresponding author at present address: Hacettepe University, Faculty of Pharmacy, Department of Pharmaceutical Chemistry, 06100 Sihhiye, Ankara, Turkey. Tel.: +90 3123051872; fax: +90 3123114777; e-mail: myarim@hacettepe.edu.tr

0968-0896/$ - see front matter © 2004 Elsevier Ltd. All rights reserved.
doi:10.1016/j.bmc.2004.10.009

to extrapolate quantitative structure–activity relationships (QSARs)[8–10] for known Oatp/OATP substrates.

In this study, we used apparent affinity (K_m) values of known Oatp1a5 substrates to perform 2D/3D-QSAR analysis. We carried out comparative molecular field analysis (CoMFA),[11] a 3D-QSAR technique that is able to yield a predictive description of global structural requirements for interactions between substrates and transport proteins. We tested the obtained model experimentally with predicted potentially new substrates using Oatp1a5 expressing MDCK cells.

2. Results and discussion

The three-dimensional structure of Oatp1a5, a multispecific transmembrane transport protein, is not available yet and the molecular basis of its multispecificity is unknown. Consequently, 2D- and 3D-QSAR studies are limited to ligand-based modeling techniques such as the classical linear multiparameter correlation approach or CoMFA. In particular, CoMFA is successfully used in drug discovery to rationalize and quantitatively predict binding activities. In the present work we have used both 2D- and 3D-QSAR (CoMFA) strategies to generate a quantitative model able to describe the important chemical features that correlate with the transport activity of Oatp1a5. A total of 18 heterogeneous compounds were included in the training set (Fig. 1; Table 1). These training set compounds contained both high and low affinity Oatp1a5 substrates with apparent K_m values between 4.3 and 417 μM as tested previously.[4,5,7] Compounds with highest affinities for Oatp1a5 include several bile salts and the thyroid hormone thyroxine whereas the steroid hormone conjugates dehydroepiandrosterone sulfate and estrone-3-sulfate and the endothelin receptor antagonist BQ-123, a cyclic pentapeptide, are typical low affinity substrates of Oatp1a5 (Table 1).

2.1. 2D-QSAR model evaluation

Correlation analysis between binding affinity (expressed as $-\log K_m$) and molecular descriptors was carried out on the training set compounds by classical linear regression multiparameters analysis. Twenty-two diverse 2D- and 3D-molecular descriptors related to physicochemical properties were computed by MOE. In order to avoid multicollinearity, 11 descriptors were removed by correlation analysis in between input variables (molecular descriptors) using dataFOREST.[†]

The variability in the biological activity parameter $-\log K_m$ was best explained by using in tandem SLog P (log of the *n*-octanol/water partition coefficient, including implicit hydrogen's) and ASA_H (water accessible surface area of all hydrophobic atoms) descriptors. The corresponding cross-validated r^2 is equal to 0.71. The relative contributions of the SLog P and ASA_H are 73.9 and 26.1, respectively. The linear response surface of $-\log K_m$ versus molecular descriptors (SLog P and ASA_H) is shown in Figure 2. Even if SLog P and ASA_H descriptors are able to describe more than 70% of the variability of our biological activity parameters, we cannot consider this QSAR as a robust quantitative model. Moreover, at the molecular fragment level, it is very difficult to rationalize which molecular features are really crucial for a compound to be transported by Oatp1a5. To improve our quantitative model, we decided to carry out a CoMFA analysis.

2.2. Alignment procedure and pharmacophore mapping

The 3D-structure alignment of the test set molecules is the most crucial step of a CoMFA analysis, since the bioactive conformation of each compound is not obvious. Consequently, alignment methodologies are usually based on a pharmacophore hypothesis. In the present study, we used the GASP (Genetic Algorithm Similarity Program) protocol to perform structure superposition. GASP uses a genetic algorithm to discover the correspondence between functional groups in different molecules and the alignment of these groups in a common geometry. Unlike methods that are limited to a precomputed set of rigid conformers, GASP allows full conformational flexibility of ligands. The program requires no advance knowledge of key functional groups or predefined correspondences between functional groups in different ligands.

By defining one molecule as a rigid template, GASP can test the fit of ligands to an existing pharmacophore model, or align molecules for constructing predictive structure–activity models using QSAR with CoMFA. A stepwise alignment procedure was applied because GASP can only handle up to six or seven molecules simultaneously, but the best strategy is to build up a series of models based on a few compounds (two or three) and compare them using the rigid template feature.[12] Compounds were compared pairwise with cholate as a template in the 'flexible alignment' approach by GASP. Using cholate as the template structure, 10 alignments per compound were generated and the one with the highest leave-one-out cross-validated r^2_{cv} value was selected from CoMFA analysis. GASP was an appropriate alignment tool for our study, as it was able to provide reasonable superposition of cholate, prostaglandin E_2, thyroxine, BSP, BQ-123, and DPDPE. As a consequence of the GASP superposition, a hypothetical pharmacophore model was proposed (Fig. 3). Three important chemical features seem to be conserved in almost all analyzed Oatp1a5 substrates (Fig. 3): (a) a negatively charged group located in the region corresponding to the carboxylic group of cholate (our reference compound); (b) a relatively extended hydrophobic region corresponding to the steroid moiety of cholate; and (c) a hydrogen bond donor in the position corresponding to the 3-OH group of cholate. Based on these findings one would predict that a potential new substrate of Oatp1a5 should exhibit a higher apparent affinity value if it contains all of these three characteris-

[†] Yamatake Corporation, 1-12-2 Kawana, Fujisawa-shi, Kanagawa 251-8522, Japan.

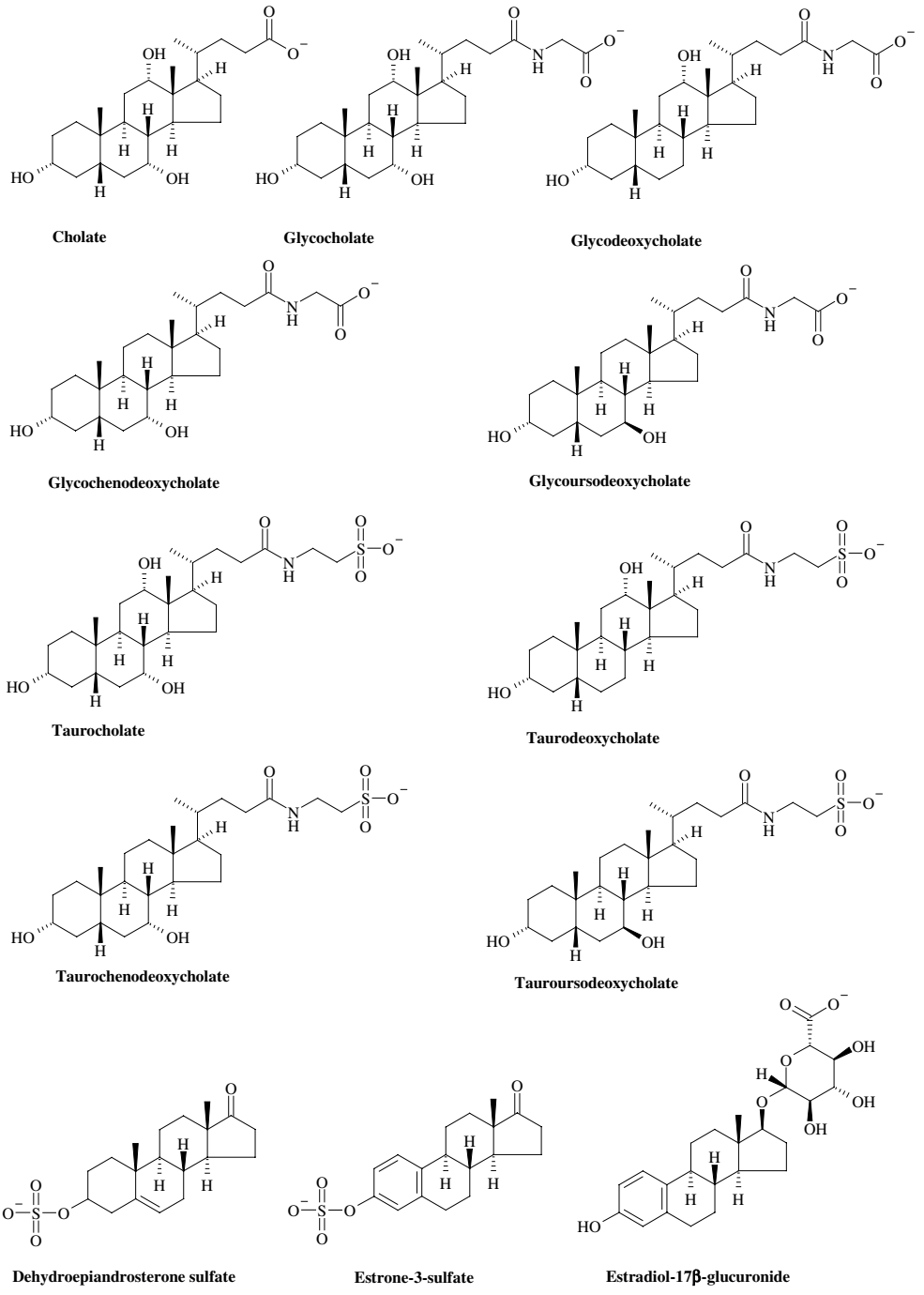

Figure 1. Molecular structures of Oatp1a5 substrates in the training set.

tics than a substrate that does only partially fit these features.

2.3. CoMFA of Oatp1a5 binding affinity

Partial least squared (PLS) regression analysis was used in conjunction with cross-validation to obtain the optimal number of components to be used in the subsequent analyses. PLS regression analysis based on least square fit gave a correlation with a cross-validated r^2_{cv} of 0.706, with the maximum number of components set equal to 3 (maximum number of components set equal to 2, 4, or 5 gave unreliable cross-validated r^2_{cv}) and the cross-validation groups set equal to the number of observations (rows) in the data table (Table 2). In order to obtain statistical confidence limits, the non-cross-validated analysis (r^2 of 0.949 (PC = 3), SEE = 0.163, F = 87.325, steric contribution = 0.491, and electrostatic contributions = 0.509) was repeated with 10 bootstrap groups, which yielded an r^2_{bs} of 0.937 (PC = 3), SEE = 0.145, Std Dev = 0.047, steric contribution = 0.487, and electrostatic contributions = 0.513 (Table 2).

The CoMFA-derived QSAR of the Oatp1a5 substrates exhibited a good cross-validated correlation, indicating that it was highly predictive. Cross-validation provides

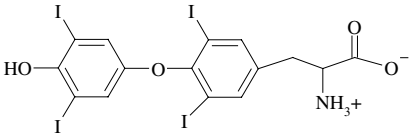

Thyroxine

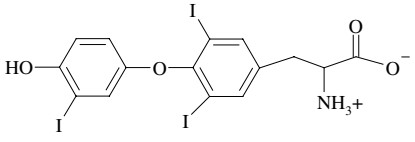

Triiodothyronine

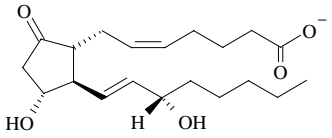

Prostaglandin E2

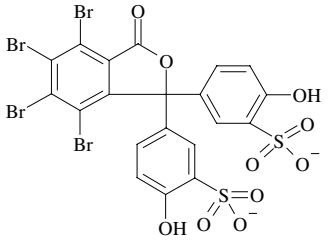

Bromosulfophtalein (BSP)

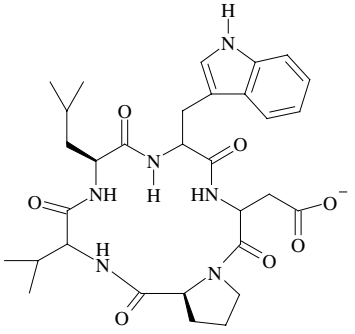

Cyclo(-D-Trp-D-Asp-Pro-D-Val-Leu-) (BQ123)

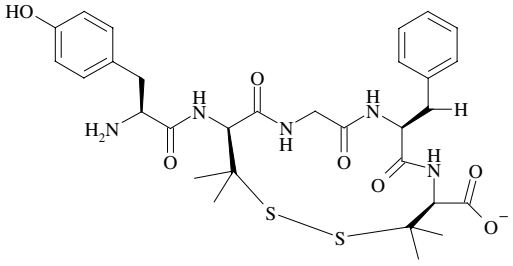

D-penicillamine2,5-enkephaline (DPDPE)

Figure 1 (*continued*)

Table 1. Substrates of Oatp1a5 and their K_m ($-\log K_m$) values

Substrates of Oatp1a5	K_m (μM)	$-\log K_m$ (μM)	Expression system	Ref.
Glycodeoxycholate	4.3	−0.63	MDCK	5
Thyroxine	5.0	−0.70	Oocytes	7
Glycoursodeoxycholate	5.3	−0.72	MDCK	5
Glycochenodeoxycholate	5.6	−0.75	MDCK	5
Taurodeoxycholate	5.8	−0.76	MDCK	5
Tauroursodeoxycholate	6.6	−0.82	MDCK	5
Taurochenodeoxycholate	7.0	−0.84	MDCK	5
Triiyodothyronine	7.0	−0.84	Oocytes	7
Bromosulfophtalein (BSP)	8.3	−0.92	Oocytes	7
Cholate	8.8	−0.94	MDCK	5
Glycocholate	15.4	−1.19	MDCK	5
Taurocholate	20.9 (18)	−1.32	MDCK (Oocytes)	5 (6)
Prostaglandin E_2	35.0	−1.54	Oocytes	7
Estradiol-17β-glucronide	39.0	−1.59	Oocytes	7
D-Penicillamine2,5-enkephaline (DPDPE)	137	−2.13	Oocytes	7
Dehydroepiandrosteron sulfate	162.2	−2.21	Oocytes	7
Estron-3-sulfate	268.8	−2.43	Oocytes	7
Cyclo(-D-Trp-D-Asp–Pro-D-Val-Leu-) (BQ-123)	417	−2.62	Oocytes	7

information concerning the predictive ability of the QSAR dataset by minimizing the occurrence of chance correlations in the QSAR model. The high bootstrapped r^2_{bs} value of 0.935 and the small standard deviation suggest a high degree of confidence in the analysis. Using this QSAR model, the apparent affinity values of the training set compounds were predicted and plotted against the experimental values (Fig. 4). The good quality of the model is demonstrated by the high correlation between prediction and experimental validation.

To visualize the model, the coefficients corresponding to each sampled field point in the resulting correlation equation were graphically plotted. Contours corre-

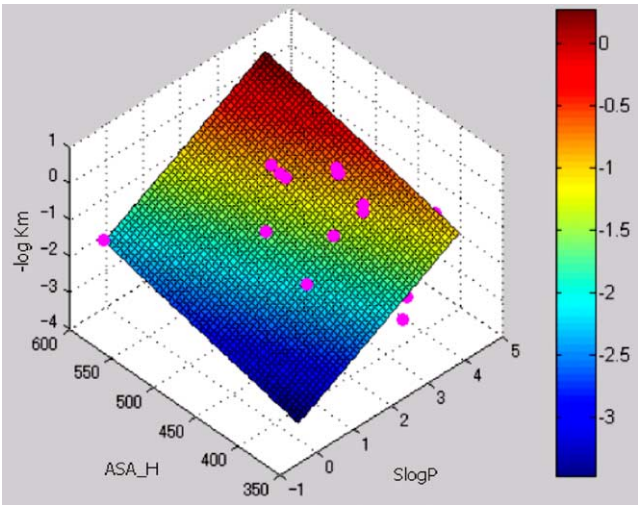

Figure 2. Response surface of $-\log K_m$ versus molecular descriptors (SLog*P* and ASA_H); ● Experimental data.

Table 2. Results obtained with the CoMFA model

Method	CoMFA
r^2_{cv}	0.705
r^2	0.949
r^2_{bs}	0.935
PC	3
SEE[a]	0.163
F	87.163
SEE[b]	0.146
Std Dev[b]	0.163
Contribution[b]	
Steric	0.486
Electrostatic	0.514

Note: r^2_{cv}, the leave-one-out (LOO) cross-validated r^2 value; r^2, no-cross-validated regression coefficient; r^2_{bs}, the cross-validated r^2 value after bootstrapping; PC, number of optimal components; SEE, standard error of estimate; *F*, *F*-statistic for analysis; Std Dev, standard deviation.

[a] After no-cross-validated regression.

[b] After bootstrapping regression.

sponding to the steric (green and yellow) and electrostatic (blue and red) fields are plotted together with glycodeoxycholate, the substrate with the highest apparent affinity, and BQ-123, the substrate with the lowest apparent affinity in Figure 5. The polyhedra describe the regions of space where the steric and the electrostatic fields are predicted to have large effect on the apparent binding affinity. The yellow and the blue polyhedra correspond to regions of the field that decrease the substrate affinity, whereas the green and the red regions increase the affinity. The negative CoMFA region is localized in the space where most test substrates contain a negatively charged group. The red polyhedra correspond to this space and indicate the area where high electron density increases the apparent affinity. It is located around the free carboxylic acid or sulfate groups in the cholic acid analogues, estradiol-17β-glucuronide, thyroxine, triiodothyronine, prostaglandine E_2, and BSP. Groups with high electron density in these areas seem to be necessary for a good interaction with the transporter polypeptide probably via positively charged amino acid side chains. The introduction of steric bulk at the side chain can have a positive effect on apparent binding affinity. Lack of negative charged and bulky groups in this area diminish the apparent affinity for the transporter. Thus, estron-3-sulfate and dehydroepiandrosterone sulfate with a negatively charged sulfate group and DPDPE and BQ-123 with a negatively charged carboxyl group in the positive CoMFA region have by far the lowest apparent affinities in the whole training set. The position of the negative group seems therefore to be of vital importance. A charged subunit introduced far beyond the red polyhedra leads to a dramatic decrease in the apparent affinity.

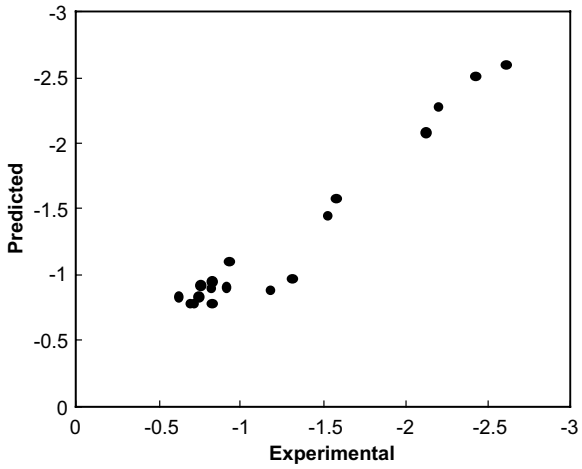

Figure 4. Graphical representation of the cross-validated predictions for the compounds in the training set. Experimental (actual) versus predicted (calculated) activity ($-\log K_m$) for the CoMFA model.

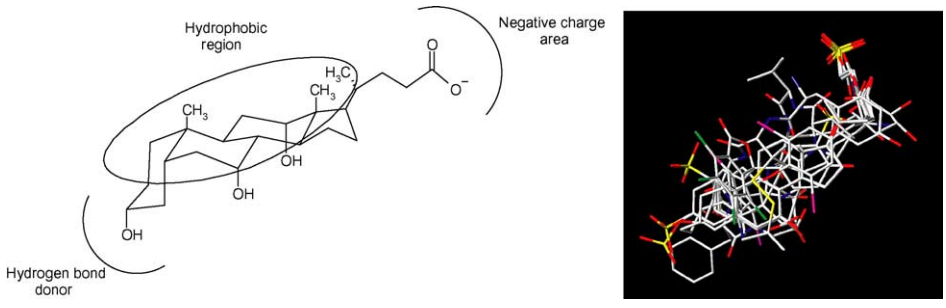

Figure 3. Pharmacophore features exemplified by cholate and the alignment of the training set compounds.

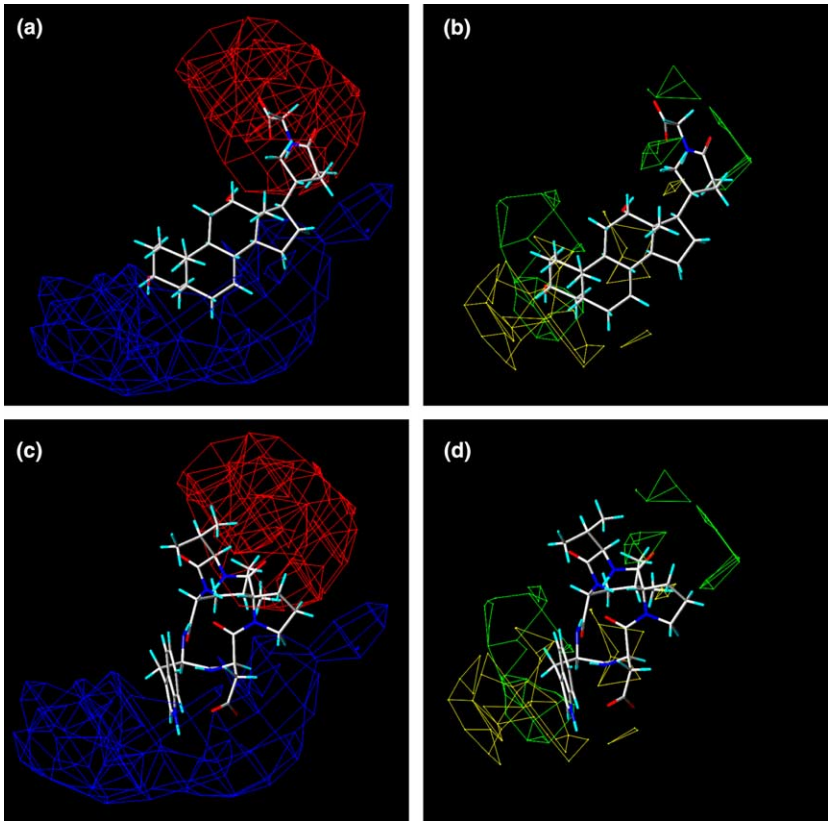

Figure 5. CoMFA Std Dev*Coeff plots for Oatp1a5 substrates denoting steric and electrostatic features. Glycodeoxycholate and BQ123 are shown within the fields (a,b) and (c,d), respectively. Green areas show regions where steric bulk enhances binding affinity, whereas yellow areas show regions where steric bulk has got a detrimental effect on binding affinity. Blue contoured areas show positively charged regions, whereas red areas show negatively charged regions.

2.4. Validation of the CoMFA model for potentially new Oatp1a5 substrates

Test compounds (Fig. 6) were used to evaluate the predictive power of this CoMFA model. The seven new potential substrates (test set compounds) were selected by chemical similarities with the training set compounds. Because we did not have radiolabeled test set compounds to directly measure Oatp1a5-mediated transport, we determined inhibition kinetics of Oatp1a5-mediated taurocholate transport. Assuming competitive inhibition, which is reflected by decreased apparent K_m and unchanged V_{max} values with increasing inhibitor concentrations, the determined K_i values should be comparable to the calculated apparent K_m values. All compounds were able to inhibit taurocholate transport. Inhibition by ursodeoxycholic acid, oleic acid, cortisol, GW4064, and dexamethasone was competitive (data not shown) while arachidonic acid and β-estradiol inhibited Oatp1a5-mediated taurocholate transport in a none competitive way. A plot of the experimentally determined K_i values ($-\log K_i$) of the five competitive inhibitors against the calculated and thus predicted apparent K_m values ($-\log K_m$) resulted in a good correlation (Fig. 7). For all five compounds the predicted apparent K_m values were slightly higher than the experimentally observed values (Fig. 7, Table 3). Thus, assuming competitive inhibition we can predict potential new Oatp1a5 substrates with our CoMFA model. Further experiments are required to directly determine whether these compounds are true transport substrates of Oatp1a5 or only inhibitors. The fact that arachidonic acid and β-estradiol do not inhibit competitively supports the previous observation of Sugiyama et al.[13] who used kinetic analysis of rat Oatp1a4-mediated transport to suggest different substrate binding sites on rat Oatp1a4. Furthermore, our results obtained with Oatp1a5 suggest that multiple substrate interaction sites might be the molecular basis of the multispecificity observed for all members of the OATP1 family.[2]

3. Conclusion

We have successfully applied the CoMFA method to a set of Oatp1a5 substrates. The resulting 3D-QSAR models show good correlations between steric and electrostatic fields and binding affinities. The CoMFA coefficient contour plots provide a self-consistent picture of the main chemical features responsible for the pK variations, and the CoMFA QSAR equations result in predictions, which agree with the experimental values. The predicted GW4064, unsaturated long chain fatty acids oleic acid, and arachidonic acid might represent a new OATP/Oatp-substrate class and could be physiological substrates of Oatp1a5.

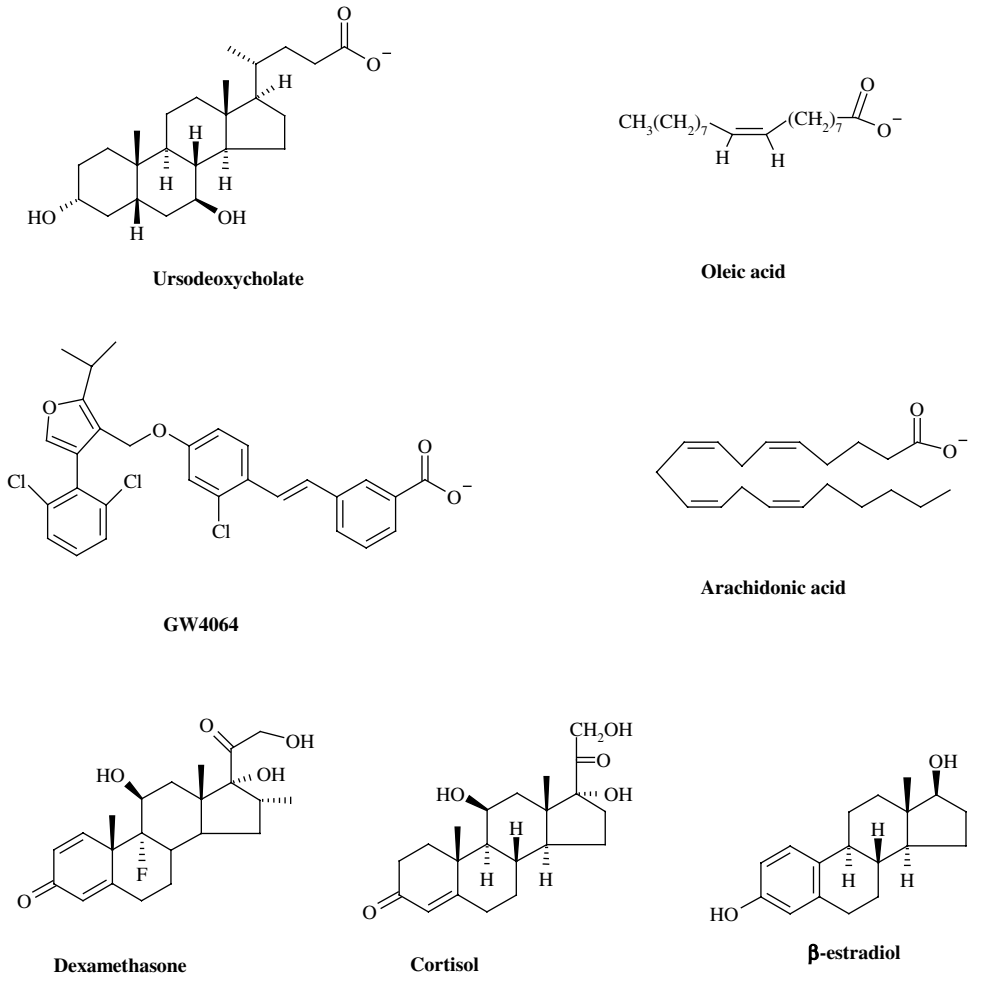

Figure 6. Molecular structures of the test set compounds.

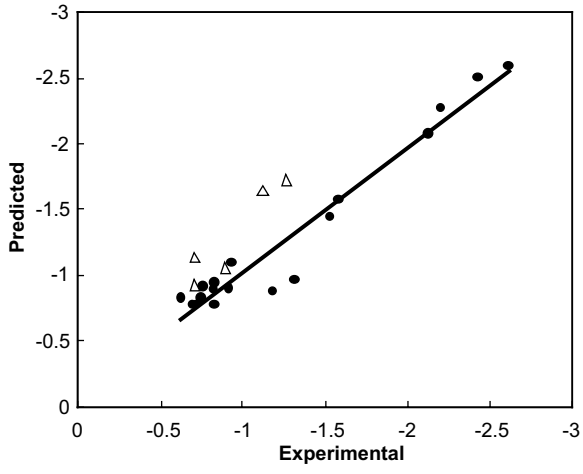

Figure 7. Experimental versus predicted activity ($-\log K_m$) for the training set compounds (●) and the test set compounds (△) with the CoMFA model.

Current information regarding the molecular and cellular aspects of drug transporters has grown steadily and encouraged studies of the mechanisms of drug absorption, distribution, and excretion. Clarification of the role of each transporter in drug excretion/detoxification in vivo is of potential importance and the elucidation of the molecular mechanisms of the multispecificity might lead to the more efficient development of safer and more effective drugs.

Table 3. Predicted and observed binding affinities for the test set compounds

Compounds	Binding affinity		Residual (log)
	Predicted ($-\log K_m$)	Observed ($-\log K_i$)	
Ursodeoxycholic acid	11.50 (−1.06)	7.88 (−0.90)	0.16
Oleic acid	8.51 (−0.93)	5.14 (−0.71)	0.22
GW4064	13.46 (−1.13)	5.08 (−0.71)	0.42
Cortisol	53.70 (−1.73)	18.66 (−1.27)	0.46
Dexamethason	44.98 (−1.65)	10.80 (−1.03)	0.62

4. Materials and methods

4.1. Computational approach

Molecular modeling and CoMFA studies were performed on a Silicon Graphics Power Graphics

O_2/R10000 workstation running SYBYL 6.8.1.[14] and QSAR studies were performed on a personal computer (AMD Athlon™ Processor, 1200 MHz). Molecular descriptors were calculated using the Molecular Operating Environment suite (MOE, 2003.04)[15] and their statistical analysis was performed using Yamatake's software (dataForest and dataNesia).†

4.2. Biological data

The CoMFA models were generated with apparent K_m values of 18 heterogeneous compounds that were determined with MDCK cells or *X. laevis* oocytes expressing Oatp1a5.[4,5,7] Taurocholate had comparable apparent K_m values of 20.9 and 18 μM in MDCK cells and oocytes, respectively.

4.3. Classical QSARs

The Molecular Operating Environment suite[15] was used to compute theoretical molecular descriptors related to physicochemical properties. Twenty-two 2D- and 3D-molecular descriptors were selected to initially describe the transport activity. Descriptor cluster analysis and linear regression analysis were carried out using Time Series Data Modeling (dataFOREST) and Spline Interpolation Algorithm (dataNESIA) software implemented by Yamatake Corp.†

4.4. Compound generation and alignment procedure

The CoMFA training set compounds were constructed using SYBYL's fragment library. All the initial structures were subsequently optimized in silico using the Tripos Force Field.[16] Gasteiger and Hückel atomic charges were used during the optimization step. The Maximin2 procedure was used for energy minimization until the gradient value was smaller than 0.001 kcal/mol Å. The resulting structures were used as starting geometries for Genetic Algorithm Similarity Program (GASP) alignments with cholate as the reference substance. GASP parameters were set to the following values: population size: 125, selection pressure: 1.1, maximum number of operations: 60,000, operation increment: 6500, fitness increment: 0.02, point cross-weight: 95.0, allele mutate weight: 96.0, full mutation weight: 0.0, full cross-weight: 0.0, internal vdW contact cutoff: 0.8.

4.5. CoMFA field calculations and regression techniques

The electrostatic and steric fields were sampled along a three-dimensional lattice. The lattice consisted of 720 sample points based on a 2.0 Å lattice spacing with boundaries extending 4.0 Å beyond the largest structure in all directions. A narrower lattice spacing with 0.75 and 1.5 Å did not improve the CoMFA results. The lattice points within the union volume of the superimposed structures were dropped. The probe used to calculate the CoMFA fields consisted of a sp^3 carbon atom with a +1 charge and a van der Waals radius of 1.52 Å. The steric and electrostatic fields were calculated separately for each molecule using a Lennard-Jones 6–12 potential and a Coulombic potential with a $1/r$ distance-dependent dielectric, respectively. The steric and electrostatic energies were truncated at 30 kcal/mol. The field values corresponding to the 720 sample points for each molecule, together with binding affinity data, were stored in a SYBYL Molecular Spreadsheet to facilitate statistical analysis.

Partial least squared (PLS) regression analysis was performed on the dataset using a subset of CoMFA field sample points falling within a standard deviation $\leqslant$1.0 kcal/mol. The steric and the electrostatic fields were scaled to equalize their weighting in the CoMFA models (SYBYL command 'scaling CoMFA_std'). PLS regression analysis was performed using cross-validation to evaluate the predictive ability of the CoMFA models. The optimal number of latent variables was derived from the cross-validation equation having the lowest standard error. A significance level $\geqslant$99.5% was estimated using the stepwise F-test. Bootstrap analysis of the dataset was used to evaluate the statistical confidence limits of the results. A σ value of 2.0 was adopted for both the cross-validated and non-cross-validated analysis. σ values of 1.0 or 0.5 did not significantly change the calculated r^2.

Initial PLS regression analysis were performed in conjunction with the cross-validation (leave-one-out method) option to obtain the optimal number of components to be used in the subsequent analysis of the dataset. The PLS regression analysis was repeated with the number of cross-validation groups set to zero. The optimal number of components was designated as that which yielded the highest cross-validated r^2_{cv} values in the non-cross-validated (conventional) analyses. The final PLS regression analysis with 10 bootstrap groups and the optimal number of components was performed on the complete dataset.

The corresponding calibration equation (resulting from the simultaneous contribution of all the observations) was derived after the optimal dimensionality of each receptor-model was established, by PLS regression analysis and cross-validation. The calibration equation with latent variables was then converted to the original parametric space represented by probe–ligand interaction energies. A 3D-QSAR was therefore derived whose coefficients were associated with statistically significant lattice locations. CoMFA coefficient contour maps were generated by interpolation of the pairwise products between the 3D-QSAR coefficients and the standard deviations of the associated energy variables.

4.6. Test set compounds and determination of K_i values

The test set consisted of seven molecules (Fig. 6). These structures were chosen to maximize a uniform sampling of biological activity. All predicted apparent K_m values were calculated using the optimized CoMFA model.

Transport of [^{3}H]taurocholic acid (129.5 GBq/mmol obtained from NEN Life Science Products AG, Boston, MA) was measured with Oatp1a5-expressing MDCK cells (kindly provided by Dr. Paul Dawson, Wake For-

est University, NC). Apparent inhibition constants (K_i values) were determined under initial rate conditions (2 min uptake values) using increasing concentrations of taurocholate (5–100 μM) in the absence or presence of inhibitors. Cells were induced 24 h before uptake determinations with 10 mM sodium butyrate. Uptake conditions were as described.[5] K_i values were calculated from three or four different experiments using the formula:

$$K_i = \frac{[I]}{\left(\frac{K'_m}{K_m} - 1\right)}$$

where [I] represents the inhibitor concentration, K_m the apparent affinity constant in the absence of inhibitor, and K'_m the apparent affinity constant in the presence of inhibitor.

Acknowledgements

We gratefully acknowledge Dr. Daniel Berger (Glaxo-SmithKline-UK) for the gift of GW4064 compound. Supported by grants 3100A0-100786/1 (to B.H.) and 31-64140.00 (to P.J.M.) from the Swiss National Science Foundation.

References and notes

1. Mizuno, N.; Niwa, T.; Yotsumoto, Y.; Sugiyama, Y. *Pharmacol. Rev.* **2003**, *55*, 425.
2. Hagenbuch, B.; Meier, P. J. *Pflugers Arch.* **2004**, *447*, 653.
3. Hagenbuch, B.; Meier, P. J. *Biochim. Biophys. Acta* **2003**, *1609*, 1.
4. Walters, H. C.; Craddock, A. L.; Fusegawa, H.; Willingham, M. C.; Dawson, P. A. *Am. J. Physiol. Gastrointest. Liver Physiol.* **2000**, *279*, G1188.
5. Abe, T.; Kakyo, M.; Sakagami, H.; Tokui, T.; Nishio, T.; Tanemoto, M.; Nomura, H.; Hebert, S. C.; Matsuno, S.; Kondo, H.; Yawo, H. *J. Biol. Chem.* **1998**, *273*, 22395.
6. Dresser, G. K.; Bailey, D. G.; Leake, B. F.; Schwarz, U. I.; Dawson, P. A.; Freeman, D. J.; Kim, R. B. *Clin. Pharmacol. Ther.* **2002**, *71*, 11.
7. Cattori, V.; van Montfoort, J. E.; Stieger, B.; Landmann, L.; Meijer, D. K. F.; Winterhalter, K. H.; Meier, P. J.; Hagenbuch, B. *Pflügers Arch.* **2001**, *443*, 188.
8. Kubinyi, H. In *3D-QSAR in Drug Design Vol. 1: Theory Methods and Applications*; Kluwer/Escom: Dordrecht, 1993.
9. Kubinyi, H.; Folkers, G.; Martin, Y. C. In *3D-QSAR in Drug Design Vol. 2: Ligand–Protein Interactions and Molecular Similarity*; Kluwer/Escom: Dodrecht, 1997.
10. Kubinyi, H.; Folkers, G.; Martin, Y. C. In *3D-QSAR in Drug Design Vol. 3: Recent Advances*; Kluwer/Escom: Dodrecht, 1998.
11. Cramer, R. D., III; Patterson, D. E.; Bunce, J. D. *J. Am. Chem. Soc.* **1988**, *110*, 5959.
12. SYBYL Molecular Modeling Software, v. 6.8.1, *Theory Manual*: Tripos Inc., 1699 South Hanley Rd, Suite 303, St. Louis, MO 63144.
13. Sugiyama, D.; Kusuhara, H.; Shitara, Y.; Abe, T.; Sugiyama, Y. *Drug Metab. Dispos.* **2002**, *30*, 220.
14. SYBYL V. 6.8, Tripos Associates, Inc., St. Louis, MO, USA.
15. Molecular Operating Environment (MOE 2002.03), Chemical Computing Group, Inc, 1255 University St., Suite 1600, Montreal, Quebec, Canada H3B 3X3.
16. Clark, M.; Cramer, R. D. I.; Van Opdenbosch, N. *J. Comput. Chem.* **1989**, *10*, 982.